https://doi.org/10.15407/ujpe66.12.1063

S. BERRI [1, 2]

[1] Department of Physics, Faculty of Science, University of M'sila
(M'sila, Algeria)

[2] Laboratory for Developing New Materials and Their Characterizations, University of Setif 1
(M'sila, Algeria)

$CsPd_{0.875}Cr_{0.125}I_3$: PROMISING CANDIDATE FOR THERMOELECTRIC APPLICATIONS

We study the electronic structure, magnetization, and thermoelectric properties of $CsPd_{0.875}Cr_{0.125}I_3$ obtained by doping $CsPdI_3$ with atoms of the 3d transition metal Cr. By applying the generalized-gradient-approximation (GGA) and the GGA + U one, we found that $CsPd_{0.875}Cr_{0.125}I_3$ alloy exhibits a completely metallic characteristic. Changes in the thermoelectric properties of the alloy are determined with the use of the BoltzTrap code. The electronic thermal conductivities (k/τ), Seebeck coefficients (S), power factors (PF), and electrical conductivities (σ/τ) are calculated. The value of the ZT merit factor is near 1 at room temperature, by indicating that $CsPd_{0.875}Cr_{0.125}I_3$ is a good candidate for thermoelectric applications at high and low temperatures.

Keywords: thermoelectric, perovskite, solar cell, DFT, magnetic materials.

1. Introduction

Perovskites are vastly studied materials due do their extensive variety of propititud physical properties, including those for spintronics and superconductivity ($CH_3NH_3PbI_{3-x}Cl_x$) [1], solar cells $(FA)_y(MA)_{1-y}PbBr_xI_{3-x})$ [2], multiferroicity ($BiFe_{1-y}Sc_yO_3$) [3], and colossal magnetoresistance ($RE_{1-x}AE_xMnO_3$ (RE = La, Pr, Sm, *etc.* and AE = = Ca, Sr, Ba,Pb)) [4].

The power conversion efficiency of perovskite-based solar cells is now becoming comparable to that of silicon photovoltaics, which is employed in the first successful experimental implementation of halide perovskite materials in solar cells by Kojima *et al.* [5]. Compared to other twenty-eight conventional solar cell materials, they provide the lowest cost in the solar energy technology [6–8]. In 2012, researchers first discovered how to make a stable, thin-film perovskite solar cell with light photon-to-electron conversion efficiencies over 10%, using lead halide peroviskites as the light-absorbing layer. Since then, the sunlight-to-electrical-power conversion efficiency of perovskite solar cells has skyrocketed, with the laboratory record standing at 25.2% [9]. Researchers are also combining perovskite solar cells with conventional silicon solar cells, whose record efficiencies for these "perovskite on silicon" tandem cells are currently 29.15% [10] (surpassing the record of 27% for conventional silicon cells) and rise rapidly. With this rapid surge in cell efficiency, perovskite solar cells and perovskite tandem solar cells may soon become cheap, highly efficient alternatives to conventional silicon solar cells [10–12].

Perovskite semiconductors offer an option that has the potential to rival the efficiency of multijunction solar cells [13], but can be synthesized under more common conditions at a greatly reduced cost. Rivaling the double, triple, and quadruple solar cells, there are all-solar cells with a max power conversion efficiency of 31.9% [14], all-perovskite triple-junction cell

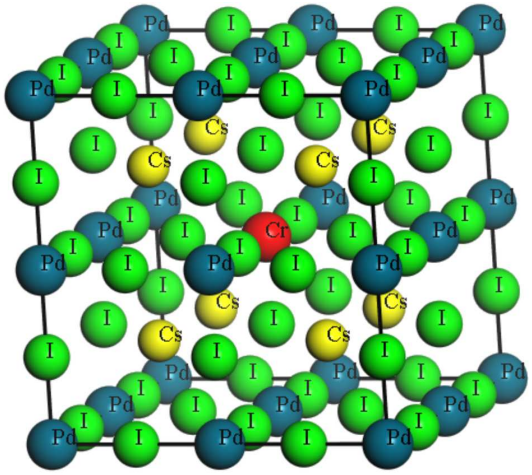

Fig. 1. Crystal structure of $CsPd_{0.875}Cr_{0.125}I_3$

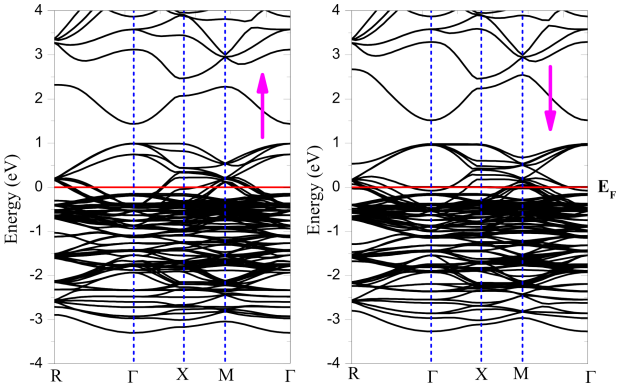

Fig. 2. Band structure for high-symmetry directions in the Brillouin zone for $CsPd_{0.875}ir_{0.125}I_3$ using the GGA + U method

reaching 33.1% [15]. These multijunction perovskite solar cells, in addition to being available for cost-effective synthesis, also maintain a high power conversion efficiency under varying weather extremes making them utilizable world wide [16].

Until know, due to their extraordinary features, the perovskite groups are received much attentions, particularly by theoretician workers [17–28]. Nevertheless, although large efforts were spent on different perovskite compounds [29–37], we need the clarification and identification of the fundamental physical characteristics of alloys. For that purpose, the current contribution reports on the electronics, magnetism, and thermoelectric properties of Cr-doped $CsPdI_3$. The computations are performed using *ab initio* calculations based on the density functional theory (DFT) within the GGA-PBE and GGA+U. More details about the methods used are given in the following section.

2. Computational Method

The considered CsPdI3 is presumed to have the ideal cubic perovskite structure (#221). The computations are based on the super cell (i.e., $2 \times 2 \times 2$) in which the Pb atom that is at (0.5, 0.5, 0.5) site in the super cell cubic structure of CsPdI3 is replaced by Cr atoms, respectively. We have established an elementary crystal structure which contains 40-atoms. The positions of the atoms during the relaxation are establish to correspond to the cubic symmetry of the space group PM-3M(n°221). The structure of the crystal for the $Pd_{0.875}Cr_{0.125}I_3$ material is shown in Fig. 1. We have used the full-potential linearized augmented plane wave (FP-LAPW) as implemented in the WIEN2K code [38]. To include the exchange-correlation part in the total electronic energy, the revised Perdew–Burke–Ernzerhof scheme within the GGA [39] is used. The Cr 3d is described through the use of the GGA + U approach [40]. This method uses an effective parameter, $U_{\text{eff}} = U + J$, in which U represents the Hubbard parameter, and J represents the exchange parameter. The Hubbard parameter approach, which includes the exchange-correlation potential, is also very efficient to study strongly correlated electrons, in which the band-gap of the given materials could be found more precisely. Then, foo such cases, we took the core electrons as relativistic, while the valence electrons are taken to be semirelativistic. These assumptions seem to be more accurate for the present method and for the full potential system. We considered the U_{eff} value as 4.97 eV. This is similar to those found in Refs. [41, 42].

The thermoelectric properties of $CsPd_{0.875}Cr_{0.125}I_3$ materials have been obtained, when we apply the theory of Boltzmann transport and use a BoltzTraP code [43, 44].

3. Results and Discussion

The electronic band structure and the density of states are computed using GGA and GGA + U for $CsPd_{0.875}Cr_{0.125}I_3$ along high-symmetry directions in the Brillouin zone as indicated in Figs. 2 and 3. The non-existence of a forbidden gap at the Fermi level

Individual and net magnetic moment (μ_B)

Compounds	Approximations	m_{Pd}	m_{Cr}	m_{I}	m_{Cs}	m_{int}	m_{total}
$CsPd_{0.875}Cr_{0.125}I_3$	GGA + U GGA	0.0957 0.1608	3.9214 3.8756	–0.03 –0.03	0.0055 0.0001	0.1752 0.2835	4.6021 4.5961
$BiCrO_3$ [45]	EXP	–	3.87	–	–	–	4.161
Ba_2CrTaO_6 [46]	GGA + U	–	2.391	–	–	–	3.00
$PrCrO_3$ [47]	GGA + U	–	2.34734	–	–	–	5.00003

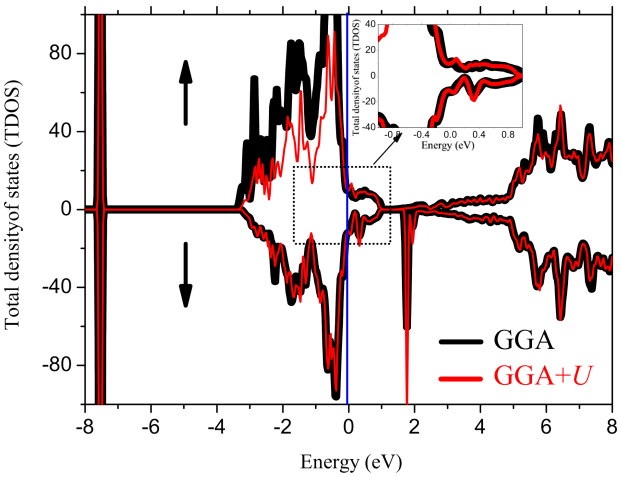

Fig. 3. Total density of states (TDOS)

oh the studied material confirms its metallic behavior indicating the existence of conductor features.

The obtained interstitial, atom-resolved and total magnetism moment of $CsPi_{0.875}Cr_{0.125}I_3$ are given in Table. The main thing, namely the total magnetic moment, is due to the Cr atoms. Small contributions come from interstitial regions and the moments of Cs, Pd, and I are negligible. The obtained data regarding the magnetic moment for Cr atoms are in agreement with those of experiment and theory cited in Refs. [45–47].

Presently, using thermoelectrics, it is possible to recapture some of the waste energy lost into the atmosphere and to convert it into electricity. The efficiency of a thermoelectric material in any power generator or cooler depends on the dimensionless constant $ZT = S^2\sigma T/\kappa$, where S is the Seebeck coefficient, σ is the electrical conductivity, κ designates the thermal conductivity, and PF is a power factor. The thermoelectric transport parameters for both pristine and doped $CsPd_{0.875}Cr_{0.125}I_3$ materials are illustrated in Figs. 4–8. $T\sigma$ is related to the temperature effect with the essential thermoelectric parameters that are (h/τ), (S), (κ/τ), the power factor $PF = S^2\sigma/\tau$, and the (ZT) factor. They have been considered in Refs. [48, 49]. The BoltzTrap code has been used to determine the thermoelectric properties; the efficiency of these properties is assessed by determining the transport parameters as functions of the temperature (T). The last coefficient characterizes the efficiency of this material, and the criterion $ZT \geq 1$ is retained in general for applications.

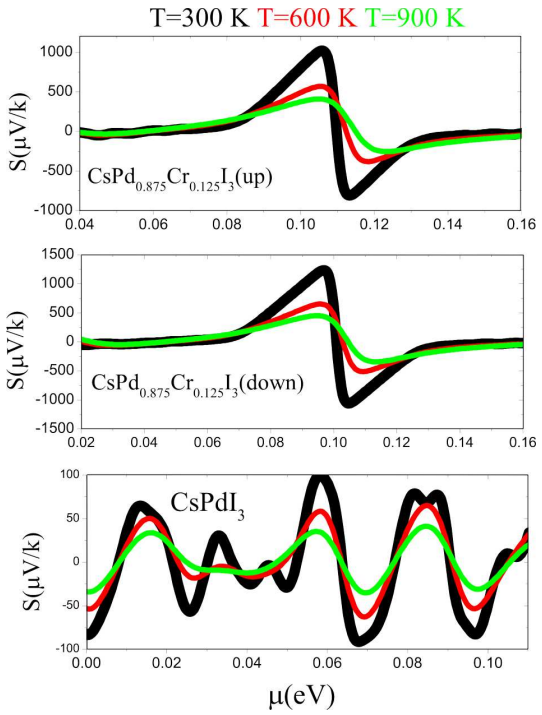

Fig. 4. SeebecK coefficient as a function of the chemical potential

The Seebeck coefficient (S) for both pristine and doped $CsPdt_3$ at three constant temperatures is

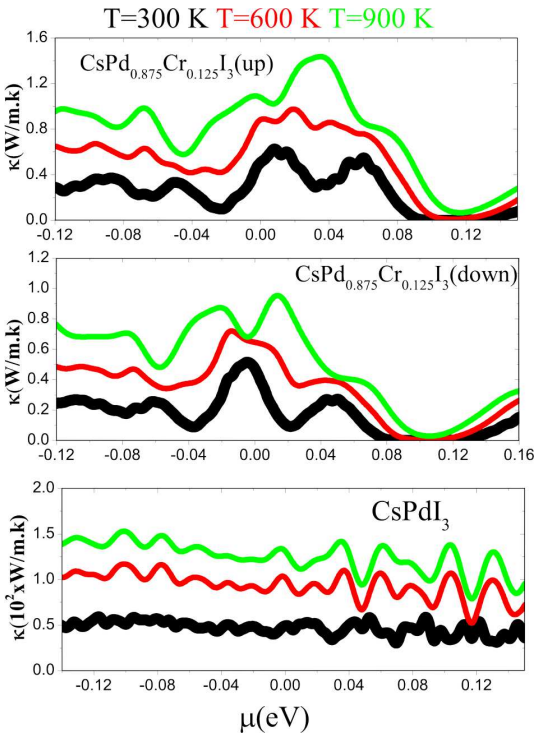

Fig. 5. Electrical conductivity as a function of the chemical potential

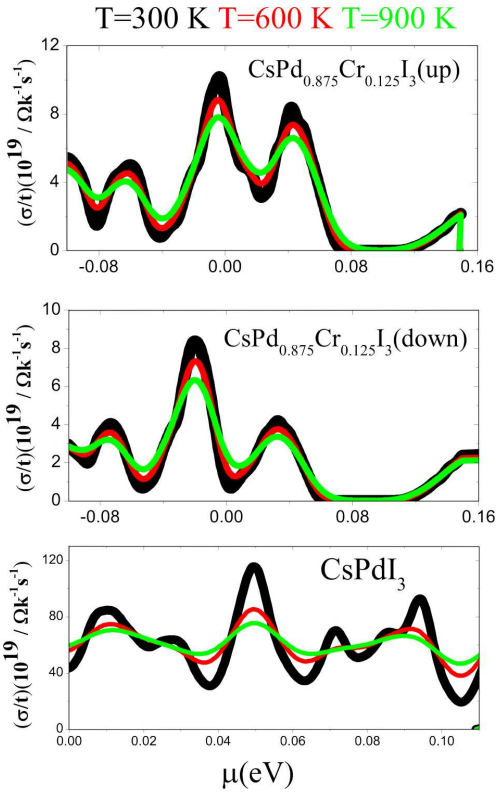

Fig. 6. Thermal conductivity as a function of the chemical potential

shown in Fig. 4. Ar 300 K, $CsPd_{0.875}Cr_{0.125}I_3$ and $CsPdI_3$ compounds of interest are remarked to have high (S) values for n-type carriers which diminish, as the temperature grows; $CsPd_{0.875}Co_{0.125}I_3$ show larger S than that of $CsPdI_3$ compound [50, 51].

The total thermal conductivity κ_e (see Fig. 5) for both pristine and doped $CsPdI_3$ includes electron κ_e and lattice κ_{lat} thermal conductivities. The value of κ_e is calculated by using $\kappa_e = LT\sigma$, where L is the Lorenz number with the standard value. We remark also that the thermal conductivity is enhanced, when the temperature is increased for $CsPd_{0.875}Cr_{0.125}I_3$ in the positive range of the chemical potential. The maxima are localized at 14.6 (900 K), 9.4 (900 K) and 151.2 (900 K) for $CsPd_{0.875}Cr_{0.125}I_3$ (up) and $CsPdI_3$ (down), respectively. Meanwhile, we can clearly seen that the thermal conductivity at room temperature is smaller than those that correspond to 600 and 900 K. Thus, the thermal properties of the material of interest are completely sensitive to the energy of solar photons. The intrinsically low thermal conductivity ($\kappa \approx 0.70$ W/mK (up) and $\kappa \approx$ ≈ 0.96 W/mK (down)) of $CsPd_{0.875}Cr_{0.125}I_3$ (up) and $CsPdI_3$ (down) is comparable to those of other materials such as $AgSbTe_2$ ($\kappa \approx 0.73$ W/mK at 600 K) [52], Ag_9TlTe_5 ($\kappa \approx 0.27$ W/mK at 600 K) [53], BiCuOSe ($\kappa \approx 0.45$ W/mK at 600 K) [54], $t_2Bi_8Se_{13}$ ($\kappa \approx 0.43$ W/mK at 600 K) [55], $Ag_4Mo_9Se_{11}$ ($\kappa \approx 0.73$ W/mK at 600 K) [56], and ($\kappa \approx 0.67$ W/mK at 600 K) of both XBi_44S_7 (X = Mn, Fe) compounds [57].

The results for the electrical conductivity (σ/τ) according to (μ) are shown in Fig. 6. It is seen that, in all cases, the temperature $T = 300$ K induces the largest electric conductivity, depicting the mobility which becomes higher at the largest temperature, by diminishing the electrical conductivity. The variation of the coefficients with a change in the chemical potential is dramatic. This indicates that the smallest carrier concentration is sufficient for achieving the efficient thermoelectric performance. The calculated electrical conductivities (σ/τ) for $CsPd_{0.875}Cr_{0.125}I_3$ (up) and $CsPdI_3$ (down) at 300 K are 10.14×10^{19} and 8.30×10^{19} $\Omega^{-1}\text{m}^{-1}\text{s}^{-1}$, respectively. By com-

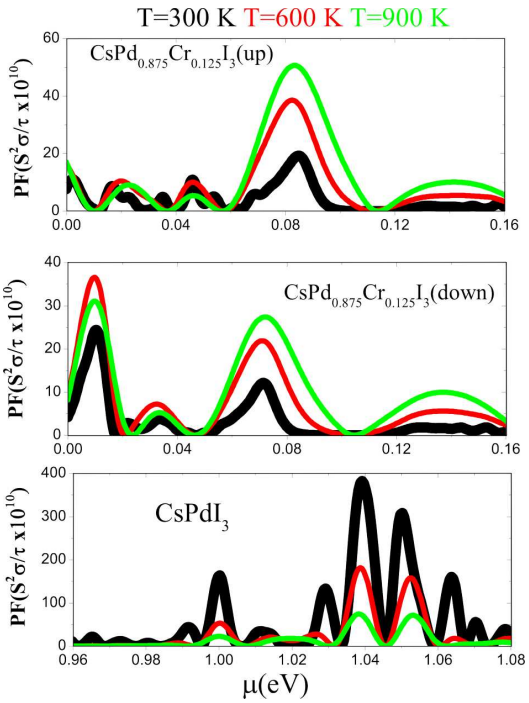

Fig. 7. Power factor ($S^2\sigma/\tau$) as a function of the chemical potential

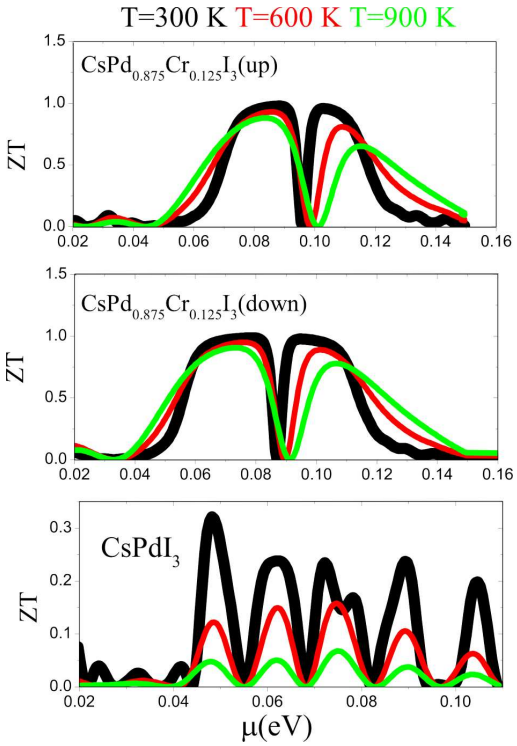

Fig. 8. Thermoelectric figure of merit (ZT) as a function of the chemical potential

paring the results on the electrical conductivity with those reported in [58–61], we found that the value of (σ/t) in our systems is higher than that found in $ts_2BiAg(Cl, Br)_6$ [58]. This may be due to the metallic character exhibited by these materials which show a lot of electron energy levels which are near the Fermi level. Some there exist a lot of electrons which are ready to move. The higher electrical conductivity for those materials induces a larger dielectric constant [62] that is important for reducing the exciton binding energy [63]. These materials can be used for solar cell applications.

We define the power factor (PF) as PF $= S^2\sigma/\tau$. Figure 7 depicts the change in PF versus (μ) and T (K). We note that the PF is augmented, when the temperature varies from 0 to 900 K. For temperatures which are smaller than 300 K, the PF rate of enhancement seems to be very moderate. However, beyond this temperature, it augments rapidly with augmenting the temperature. For PF which is lower than one, the voltage and current are not in phase. In fact, for the same amount of useful power transferred, a load with a low PF in an electric power system shows a higher current than with loads with a higher PF. By comparing the results on PF with those reported for SnSe. The PFs remain at a high value $\sim 50.60 \times 10^{10}$ and 30.34×10^{10} $(\mathrm{Wm^{-1}K^{-1}})$ around 773 K for $CsPd_{0.875}Cr_{0.125}I_3$ (up) and $CsPdI_3$ (down), which is twice higher than that of ~ 6.4 $\mathrm{Wm^{-1}K^{-2}}$ at 773 K for the SnSe [64].

To know the efficiency of a thermoelectric material, it is necessary to determine the value of ZT. In the present study, ZT contains the total thermal conductivity $\kappa = \kappa_e + \kappa_{\mathrm{lat}}$. Our calculated ZT for both pristine and doped $CsPdI_3$ are plotted in Fig. 8. The value of ZT for $CsPd_{0.875}Cr_{0.125}I_3$ (up) and $CsPdI_3$ (down) is high and almost constant up to 300 K. Then it decreases slightly, as the temperature increases. We observe that the ZT value is about 0.976 and 0.325 at room temperature for $CsPd_{0.875}Cr_{0.125}I_3$ (up) and $CsPdI_3$ (down), respectively. It turns out that these values are very high as compared to the available thermoelectric materials, and we can explain this by the high Seepeck coefficients in the studied systems. The present results also indicate the maximum potential of the $CsPd_{0.875}Cr_{0.125}I_3$ as a high temperature thermoelectric material, rather than the $CsPdI_3$. Keeping

in view the above results on thermoelectric properties, we conclude that $CsPd_{0.875}Cr_{0.125}I_3$ shows a considerable thermoelectric performance accompanied by a significant ZT which are than for many perovskite compounds reported till now. We cannot compare our results due to shortage of experimental or theoretical results. Nevertheless, these simulations can be considered as reference data for future investigations.

4. Conclusions

In the present work, the electronic, magnetic, and thermoelectric properties of $CsPd_{0.875}Cr_{0.125}I_3$ have been studied using the FP-LAPW method, in which we have applied GGA and GGA + U approximations. A metallic character has been shown by the electronic structures of the ferromagnetic configuration for $CsPd_{0.875}Cr_{0.125}I_3$ alloy. The main contribution to the magnetic moment is made by the Cr ions. High ZT values of 0.976 and 0.988 were obtained for $CsPd_{0.875}Cr_{0.125}I_3$(up) and $CsPd_{0.875}Cr_{0.125}I_3$(down), respectively. Our thermoelectric study predicts $CsPd_{0.875}$ $Cr_{0.125}I_3$ as a probable thermoelectric material with considerable values of the ZT factor at low temperatures. Finally, the investigated properties suggest the application of this material in thermoelectric devices.

1. K. Liao, X. Hu, Y. Cheng, Z. Yu, Y. Xue, Y. Chen, Q. Gong. Spintronics of hybrid organic–inorganic perovskites: Miraculous basis of integrated optoelectronic devices. *Adv. Optical Mater.* **7** (15), 1900350 (2019).
2. W. Yan, H. Rao, C. Wei, Z. Liu, Z. Bian, H. Xin, W. Huang. Highly efficient and stable inverted planar solar cells from $(FAI)_x(MABr)_{1-x}PbI_2$ perovskites. *Nano Energy* **35**, 62 (2017).
3. E.L. Fertman, A.V. Fedorchenko, E. Čižmár, S. Vorobiov, A. Feher, Y.V. Radyush, A.V. Pushkarev, N.M. Olekhnovich, A. Stanulis, A.R. Barron, D.D. Khalyavin, A.N. Salak. Magnetic diagram of the high-pressure stabilized multiferroic perovskites of the $BiFe_{1-y}Sc_yO_3$ series. *Crystals* **10** (10), 950 (2020).
4. A. Kojima, K. Teshima, Y. Shirai, T. Miyasaka. Organometal halide perovskites as visible-light sensitizers for photovoltaic cells. *J. Am. Chem. Soc* **131**, 6050 (2009).
5. Y-K. Liu, Y-W. Yin, X-G. Li. Colossal magnetoresistance in manganites and related prototype devices. *Chinese Phys. B* **22**, 087502 (2013).
6. H.J. Snaith. Perovskites: The emergence of a new era for low-cost, high-efficiency solar cells. *E. Phys. Chem. Lett.* **4** (21), 3623 (2013).
7. C. Karan, N. Mercier, J. Even. Quantum and dielectric confinement effects in lower-dimensional hybrid perovskite semiconductors. *Chem. Rev.* **119**, 3140 (2019).
8. K. Yoshikawa, H. KawaKaki, W. Yoshida, T. Irie, K. Konishi, K. Nakano, T. Uto, D. Adachi, M. Sanematsu, H. Uzu, K. Yamamoto. Silicon heterojunction solar cell with interdigitated back contacts for a photoconversion efficiency over 26%. *Nature Energy.* **2**, 17032 (2017).
9. F. Sahli, J. Werner, B.J. Kamino, M. Bräuninger, R. Monnard, B. Paviet-Salomon, L. Barraud, L. Ding, J.J. Diaz Leon, D. Sacchetto, G. Caetaneo, M. Desptisse, M. Boccard, S. Nicolay, Q. Aeangros, B. Niesen, C. Ballif. Fully textured monolithic perovskite/silicon tandem solar cells with 25.2% powef conversion efficiency. *Nat. Mater.* **17**, 820 (2018).
10. https://www.nrel.gov/pv/assets/pdfs/best-research-cell-efficiencies.20191106.pdf
11. i. Liu, M.B. Joheston, H.J. Snaith. Efficient planar heterojunction perovskite solar cells by vapour deposition. *Nature.* 501, 395 (2013).
12. J. Burhcska, N. Pellet, S-J. Moon, R. Humphry-Baker, P. Gao, M.K. Nazeeruddin, M. Gräkzel. Sequential deposition as a route to high-performance perovskite-sensitized solar cells. *Nature.* **499**, 316 (2013).
13. M.T. Hörantner, T. Lrijtens, M.E. Ziffer, G.E. Epeeon, M.G. Christoforo, M.D.'McGehee, H.J. Snaith. The potential of multijunction perovskite solar cells. *ACS Energy Letters.* **2** (10), 2506 (2017).
14. B.E. Haroin, H.J. Snaith , M.D. McGehee. The renaissance of dye-sensitized solar cells. *Nature Photon.* **6**, 162 (2012).
15. J.G. Werthen. Multijunction concentrator solar cells. *Solar Cells.* **21** (1–4), 452 (1987).
16. D.P. McMeekin, S. Mahesh, N.K. Nvel, M.T. Klug, J.C. Lim, J.H. Warby, J.M. Ball, L.M. Herz, M.B. Johniton, H.J. Snasth. Solution-processed all-perovskite multijunction solar cells. *Joule* **3** (2), 387 (2019).
17. S. Berri. First-principles study on half-metallic properties of the Sr_2GdReO_6 double perovskite. *J. Magn. Magn. Mater.* **385**, 124 (2015).
18. I. da S. Carvalho, A.J.S. Sipva, P.A.M. Nascimento, B.J.A. Moulton, M.V. dos S. Rezende. The effect of different chelating agent on the lattice stabilization, structural and luminescent properties of $Gd_3Al_5O_{12}:Eu^{3+}$ phosphors. *Optical Materials.* **98**, 109449 (2019).
19. M.H.N. Peres, P.D. Borges. Ab initio study of $Pr_{1-x}Sr_xCrO_{3-\delta}$ cubic perovskites: Solid oxide fuel cells applications. *J. Solit Stade Chem.* **290**, 121581 (2020).
20. P. Xiaokaiti, T. Yu, A. Yoshida, G. Guan, A. Abudula. Evaluation of cesium doped perovskites $(Ce_{0.1}Sr_{0.9})_xCo_{0.3}Fe_{0.7}O_{3-\delta}$ as cathode materials for rolid oxide fuel cells. *Catalysis Today* **332**, 94 (2019).
21. A. Koureche, D. Maouche, S. Berri, M. Ibrir. Ab initio prediction of structural, electronic, magnetic and optical properties of Ba_2GdSbO_6. *Mater. Sci. Semicond. Process.* **40**, 58 (2015).
22. M. Taguchi, F. Matcui, N. Maejima, H. Matsui, H. Daimon. Disorder and mixed valence properties of Sr_2FeMoO_6 studied by photoelectron diffraction and x-ray absorption spectroscopy. *Surface Sci.* **683**, 53 (2019).

23. S. Berri. Half-netallic ferromagnetism in Li_6VCl_8, Li_6MnCl_8, Li_6CoCl_8 and Li_6FeCl_8 from first principles. *J. Supercond. Nov. Magn.* 29, 2381(2016).
24. S. Berri. First-principles investigation of the physical properties of XSb_2O_6 (X = Ca, Sr, Ba) and YAs_2O_6 (Y = Mn, Co). *Comput. Condens. Matter.* **22**, e00440 (2020).
25. S. Berri, D. Maouche, Y. Medkout. Ab initio study of the strucrural, electronic and elastic properties of $AgSbTe_2$, $AgSbSe_2$, Pr_3AlC, Ce_3AlC, Ce_3Ale, La_3AlC and La_3AlN compounds. *Physica B* **407** (17), 3320 (2020).
26. M. Oumertem, D. Maouche, S. Berri, N. Bouarissa, D.P. Rai, R. Khenata, M. Ibrir. Theoretical investigation of the structural, electronic and thermodynamic properties of cubic and orthorhombic $XZrS_3$ (X = Ba, Sr, Ca) compounds. *J. Comput. Electpon.* **18**, 415 (2019).
27. S. Berri. First-principles studies of thermoelectric and thermodynamic properties of the complex perovskite $Ba_3MnNb_2O_9$. *J. Sci-Adv. Mater. Dev.* **5** (3), 378 (2020).
28. Y. Zhao, J. Du, Z. Xu. Enhanced piezoelectric properties with a high strain in $(K_{0.44}Na_{0.52}Li_{0.04})(Nb_{0.86}Ta_{0.1}Sb_{0.04})O_{3-x}$ wt% Sc_2O_3 lead-free ceramics. *Mater. Scie. Engin.: B* **224**, 110 (2017).
29. Y. Dumar, i.C. Sanal, T.K. Peruz, X. Mathew. Band offset studies of $MAPbI_3$ perovskite solar cells using X-ray photoelectron spectroscopy. *Opt. Mater.* **92**, 425 (2019).
30. S. Berri. Theoretical analysis of the structural, erectronic and optical properties of tetragonal Sr_2GaSbO_6. *Chin. J. Phys.* **55** (6), 2476 (2017).
31. J. Fan, Y. Xie, F. Qian, Y. Ji, D. Hu, R. Tang, W. Liu, L. Zhang, W. Tmng, C. Ma, H. Yang. Isotropic magnetoresistance and enhancement of ferromagmetism through repetitious bending moments in flexible perovskite manganite thin film. *J. Alloys Compd.* **806**, 753 (2019).
32. S. Berri. Ab initio study of fundamental properties of $XAlO_3$ (X = Cs, ub and K) compounds. *J. Sci.-Adv. Mater. Dev.* **3** (2), 254 (2018).
33. Y.-Y. Chin, H.-J. Lin, Z. Hu, Y. Shimakawa, C.-T. Chen. Direct observation of the partial valence transition of Cu in the A-site ordered $LaCu_3Fe_4O_{12-\delta}$ by soft X-ray absorption spectroscopy. *Physica B* **568**, 92 (2019).
34. S. Berri. Theoretical analysis of the structural, electronic, opticol and thermodynamic properties of trigonal and hexagonal $Cs_3Sb_2I_9$ compound. *Eur. Phys. J. B* **93**, 191 (2020).
35. S. Berri. Ab-initio calculations on structural, electronic, half-metallic and optical properties of Co-, Fe-, Mn- and Cr-doped Ba_2LuTaO_6. *Pramana – J. Phys.* **95**, 38 (2021).
36. S. Berri. Search for new half-metallic ferromagnets in quaternary diamond-like compounds I–II_2–III–VI_4 and I_2–II–IV–VI_4 (I = Cu; II = Mn, Fe, Co; III = In; IV = Ge, Sn; VI = S, Se, Te). *J. Supercond Nov Magn.* **31**, 1941 (2018).
37. S. Berri. First-principles search for half-metallic ferromagnetism in double perovskite X_2MnUO_6 (X = Sr or Ba) compounds. *Acta Physica Polonica, A* **138** (6), 834 (2020).
38. P. Blaha, K. Schwarz, G.K.H. Madsen, D. Kvasnicka, J. Luitz, R. Laskowski, F. Tran, L.D. Marks. *WIEN2K. An Auglented Plane Wave + Local Orbitals Program for Calculating Crystal Properties* (Techn. UniversitSt, 2001) [ISBN-3-9501031-1-2].
39. J.P. Perdew, K. Burke, M. Ernzerhof. Generalized Gradient Approximation Made Simple. *Phys. Rev. Lett.* **77**, 3865 (1996).
40. V.I. Anisimov, J. Zaanen, O.K. Andersyn. Band theory and Mott insulators: Hubbard U instead of Stoner I. *Phys. Rev. B.* **44**, 943 (1991).
41. S. Berri. First-principles calculations to investigate structural, erectronic, half-metallic and thermodynamic properties of hexagonal UX_2O_6 (X = Cr,V) compounds. *J. Sci.-Adv. Mater. Dev.* **4** (2), 319 (2019).
42. A. Souidi, S. Bentata, W. Bensttali, B. Bouadjemi, A. Abbad, T. Lantri. First principle study of spintronic properties for double perovskites Ba_2XaoO_6 with X = V, Cr and Mn. *Mater. Sci. Senicond. brocess.* **43**, 196 (2016).
43. G.K.H. Madsen, D.J. Singh. BoltzTraP. A code for calculating band-structure dependent quantities. *Comput. Phys. Commun.* **175**, 67 (2006).
44. W. Namhongsa, M. Rittiruam, K. Singsoog *et al.* Thermoelectric properties of GeTe and Sb_2Te_3 calculated by decsity functional theory. *Materials today: Proceed.* **5**, 14131 (2018).
45. A.A. Belik. Magnetic properties of solid solutions between $BiCrO_3$ and $BiGaO_3$ with perovskite structures. *Sci. Technol. Adv. Mater.* **16** (2), 026003 (2015).
46. M. Nabi, T.M. Bhat, D.C. Gupta. Effect of pressure on electronic, magnetic, thermodynamic, and thermoelectric properties of tantalum-baseg double perovskites Ba_2MTaO_6 (M = Mn, Cr). *Int. J. Eneray Res.* **43** (9), 4229 (2019).
47. M. Yaseen, H. Ambreen, J. Iqbal, A. Shahzad, R. Zihid, N.A. Kattan, S.M. Ramay, A. Mahmood. Elertronic, optical and magnetic properties of $PrXO_3$(X = V, Cr): first-principle calculations. *Philosophical Magazine* **100** (24), 3125 (2020).
48. M. Núñez-Valdez, Z. Allahyari, T. Fan, A.R. Oganov. Efficient technique for computational design of thermoelectric materials. *Comput. Phys. Commun.* **222**, 152 (2018).
49. S. Ahmad, R. Ahmad, M. Bilal, N.U. Rehman. DFT studies of thermoelectric properties of RпїSAu intermetallics at 300 K. *J. Rare Earths* **36**, 197 (2018).
50. E.M. Levin. Effects of Ge substitution in GeTe by Ag or Sb on the Seebeck coefficient and carrier concentration derived from ^{125}Te NMR. *Phys. Rev. B* **93**, 045209 (2016).
51. S. Berri, M. Attallah, N. Bouarissa, M. Ibrir. Electronic structure and thermoelectric properties of Co-, Fe-, Mn-, and Cr-doped Ba_2LuTaO_6 from spin-polarized calculations. *Phys. Status Solidi (b)* **258** (2), 2000402 (2021).
52. D.T. Morelli, V. Jovovic, J.P. Heremans. Intrinsically minimal thermal conductivity in cubic I–V–VI_2 semiconductors. *Phys. Rev. Lett.* **101**, 035901 (2008).

53. K. Kurosaki, A. Kosuga, H. Muta, M. Uno, h. Yamanaka. Mg_9TlTe_5: A high-performance thermoelectric bulk material with extremely low thermal conductivity. *Appl. Phys. Lett.* **87**, 061919 (2005).
54. J. Li, J. Sui, C. Barreteau, D. Berardan, N. Dragoe, W. Cai, Y. Pei, L-D. Zhao. Thermoelectric properties of Mg doped *p*-type BiCuSeO oxyselenides. *J. Alloys Compd.* **551**, 649 (2013).
55. Y. Pei, C. Chang, Z. Wang, M. Yin, M. Wu, G. Tan, H. Wu,Y. Chen, L. Zheng, S. Gong, T. Zhu, X. Zhao, L. Huang, J. He, M.G. Kanatzidis, L-D. Zhao. Multiple converged conduction bands in $K_2Yi_8Se_{13}$: A promising thermoelectric material with extremely low thermal conductivity. *J. Am. Chem. Soc.* **138**, 16364 (2016).
56. T. Zhou, B. Lenoir, M. Colin, A. Dauscher, R.A.R.A. Orabi, P. Gougeon, M.Potel, E. Guilmeau. Promising thermoelectric properties in $Ag_xMo_9Se_{11}$ compounds ($3.4 \leq x \leq \leq 3.9$). *Appl. Phys. Lett.* **98**, 162106 (2011).
57. J-B. Labégorre, A. Virfeu, A. Bourhim, H. Willeman, T. Barbier, F. Appert, J. Juraszek, E. Malaman, A. Huguenot, R. Gautier, V. Nassif, P. Lemoine, C. Prestipino, E. Elkaim, L. Pauyrot-d'Alençon, T. Le Mercier, A. Maignan, R.A.R.A. Orabe, E. Guilmiau. XBi_4S_7 (X = Mn, Fe): New cost-efficient layered *n*-type thermoelectric sulfides with ultralow thermal conductivity. *Adv. Funct. Mater.* **1904112**, 1 (2019).
58. E. Haque, M. A. Hossain. Origin of ultra-low thermal conductivity in Cs_2BiAgX_6 (X = Cl, Br) and its impact on thermoelectrlc performance. *J. Ailoys Compl.* **748**, 63 (2018).
59. Q. Mahmood, T.H. Flemban, H. Althib, T. Alshahrani, M.G.B. Ashiq, B. Ul Haq, Y. Tahir, A. Surrati, N.A. Kattan, A. Laref. The study of optical and thermoelectric properties of lead-free variant iodes (K/Rb) $_2TiI_6$; Renewable energy. *J. Mater. Res. Technol.* **9** (6), 13043 (2020).
60. S.A. Mir, D.C. Gupta. Understanding the origin of semiconducting ferromagnetic character along with the high figure of merit in Cp_2NaMCn_6 (M = Cr, Fe) double perovskites. *J. Magn. Magn. Mater.* **519**, 167431(2021).
61. N.A. Noor, M. Waqas Iqbal, T. Zelai, A. Mahmood, H.M. Shaikh, S.M. Ramay, W. Al-Masry. Analysis of direct band gap A_2ScInI_6 (A = Rb, Cs) double perovskite halides using DFT approach for renewable energy devices. *J. Mater. Res. Technol.* **13**, 2491 (2021).
62. J. Smit, H.P.J. Wijn. Physical properties of ferrites. *Adv. Electron. Electron Phys.* **6**, 69 (1954).
63. A.T. Hanbicki, M. Currie, G. Kioseoglou, A.L. Friedman, B.T. Jonker. Measurement of high exciton binding energy in the monolayer transition-metal dichalcogenides WS_2 and WSe_2. *Solid State Commun.* **203**, 16 (2015).
64. L-D. Zhao, G. Tan, S. Hao, J. He, Y. Pei, H. Chi, H. Wang, S. Gong, H. Xu, V.P. Dravid, C. Uher, G.J. Snyder, C. Wolverton, M.G. Kanatzidis. Ultrahigh power factor and thermoelectric performance in hole-doped single-crystal SnSe. *Science* **351** (6269), 141 (2016).

Received 21.05.21

С. Беррі

$CsPd_{0,875}Cr_{0,125}I_3$: ПЕРСПЕКТИВНИЙ КАНДИДАТ ДЛЯ ЗАСТОСУВАНЬ В ОБЛАСТІ ТЕРМОЕЛЕКТРИКИ

Вивчаються електронна структура, магнітні та термоелектричні властивості сполуки $CsPd_{0,875}Cr_{0,125}I_3$, отриманої допуванням $CsPdI_3$ атомами 3*d* перехідного металу Cr. Використовуючи узагальнене градієнтне наближення (УГН) і УГН + U, ми знаходимо, що сплав $CsPd_{0,875}Cr_{0,125}I_3$ має властивості металу. Зміни термоелектричних параметрів розраховано із застосуванням програми BoltzTrap. Обчислено електронні теплопровідності (k/τ), коефіцієнти Зеєбека (S), фактори потужності та електричні провідності (σ/τ). Розраховане значення зведеного коефіцієнта ZT знаходиться близько 1 при кімнатній температурі, вказуючи на те, що $CsPd_{0,875}Cr_{0,125}I_3$ є хорошим кандидатом для застосування в області термоелектрики при низьких і високих температурах.

Ключові слова: термоелектричний, перовскіт, сонячний елемент, теорія функціонала густини, магнітні матеріали.